

Fractional Kohn–Sham Occupancies from a Strong-Correlation Density Functional

Axel D. Becke

Abstract It is not always possible in Kohn–Sham density-functional theory for the non-interacting reference state to have integer-only occupancies. Cases of “strong” correlation, with very small HOMO-LUMO gaps, involve fractional occupancies. At the transition states of symmetric avoided-crossing reactions, for example, representation of the correct density requires a 50/50 mixing of degenerate HOMOs. In a recent paper (Becke, *J Chem Phys* 139:021104, 2013) the “B13” strong-correlation density functional of Becke (*J Chem Phys* 138:074109, 2013 and 138:161101, 2013) was shown to give excellent barrier heights in symmetric avoided-crossing reactions. However, the calculations were performed only at reactant and transition-state geometries, where the fractional HOMO-LUMO occupancies in the latter are 50/50 by symmetry. In the present chapter, we compute full reaction curves for avoided crossings in $H_2 + H_2$, ethylene (twisting around the double bond), and cyclobutadiene (double-bond automerization) by determining fractional occupancies variationally. We adopt a practical strategy for doing so which does not involve self-consistent B13 computations (not yet possible) and involves minimal cost. Single-bond dissociation curves for H_2 and LiH are also presented.

Keywords Density-functional theory · Electronic structure · Strong correlation

Contents

1	Introduction	176
2	The B13 Strong-Correlation Density Functional	178
3	Avoided-Crossing Reaction Curves	181

A.D. Becke (✉)

Department of Chemistry, Dalhousie University, 6274 Coburg Rd., P.O. Box 15000, Halifax NS, B3H 4R2, Canada

e-mail: axel.becke@dal.ca

4	H ₂ and LiH Dissociation Curves	183
5	Summary and Conclusions	185
	References	186

1 Introduction

Kohn–Sham density-functional theory (KS-DFT) is based on a non-interacting, single-Slater-determinant reference state having the *same total density* ρ as the “real” interacting system [1–3]. The KS reference orbitals ψ_i satisfy the single-particle Schroedinger equation

$$-\frac{1}{2}\nabla^2\psi_i + v_{\text{KS}}\psi_i = e_i\psi_i \quad (1)$$

where v_{KS} is the non-interacting potential such that

$$\rho = \sum_i n_i \psi_i^2, \quad n_i = 0, 1, \text{ or } 2 \quad (2)$$

equals the density of the real system. The KS potential is given by [2]

$$v_{\text{KS}} = v_{\text{ext}} + v_{\text{el}} + v_{\text{XC}}, \quad v_{\text{el}} = \int \frac{\rho(r_2)}{r_{12}} d^3r_2, \quad v_{\text{XC}} = \frac{\delta E_{\text{XC}}}{\delta \rho} \quad (3)$$

where v_{ext} is the external (one-body) potential in the real system, v_{el} is the classical Coulomb potential arising from the electron density, and v_{XC} is the functional derivative [3] with respect to the density of the “exchange–correlation” energy E_{XC} defined by

$$E_{\text{total}} = -\frac{1}{2}\sum_i n_i \int \psi_i \nabla^2 \psi_i + \int \rho v_{\text{ext}} + \frac{1}{2} \iint \frac{\rho(r_1)\rho(r_2)}{r_{12}} + E_{\text{XC}} \quad (4)$$

i.e., that part of the total energy containing all the quantum and correlation effects.

We restrict ourselves in this work to singlet states. Thus the occupation numbers n_i in (2) and (4) are 0 or 2 if the reference state is a *single* Slater determinant. Not all quantum systems, however, can be referred to a single determinant or “configuration”. Consider a four-electron system in a perfectly square D_{4h} nuclear framework: square H₄, for example, or the pi-electrons in square cyclobutadiene C₄H₄. The orbital energies are as sketched in Fig. 1, with a doubly degenerate HOMO set, ψ_a and ψ_b . Two equivalent singlet configurations (determinants) are possible: $|\psi_a^2\rangle$ and $|\psi_b^2\rangle$ in the figure. These interact strongly to produce the two-configuration mixtures Ψ_{\pm} :

Fig. 1 D_{4h} Slater determinants


$$\Psi_{\pm} = \frac{1}{\sqrt{2}}(|\psi_a^2\rangle \pm |\psi_b^2\rangle) \quad (5)$$

with Ψ_- being the ground state. Neither of the individual determinants, $|\psi_a^2\rangle$ or $|\psi_b^2\rangle$, is an adequate reference state. Indeed, neither has a density having even the correct D_{4h} symmetry of the actual ground-state density (if we constrain ourselves to *real* orbitals). The actual ground-state ρ is represented by

$$\rho = 2 \sum_{i=1}^{\text{HOMO}-1} \psi_i^2 + \psi_a^2 + \psi_b^2 \quad (6)$$

involving occupancies *other than* 2 for the degenerate HOMO orbitals. In each of ψ_a and ψ_b , there is *half* an electron of spin up and *half* an electron of spin down.

The orbital occupancies in the above example are fixed by symmetry: i.e., a doubly degenerate HOMO level yielding two symmetry-equivalent reference configurations. In general, strongly correlated systems have densities of the form

$$\rho = 2 \sum_{i=1}^{\text{HOMO}-1} \psi_i^2 + 2(1-f)\psi_{\text{HOMO}}^2 + 2f\psi_{\text{LUMO}}^2 \quad (7)$$

where f may have *any* value in the interval $0 \leq f \leq 1$, depending on the HOMO-LUMO gap and the relevant interaction matrix elements. The f parameter in (7), and the corresponding fractional occupancies in (4), must be determined variationally.

An analysis by Schipper et al. [4] of the $\text{H}_2 + \text{H}_2$ reaction is a beautiful illustration. These authors have computed accurate CI and MRCI wavefunctions at various points on the $\text{H}_2 + \text{H}_2$ potential-energy surface and, at each geometry, have extracted the exact Kohn–Sham potential v_{KS} and orbitals ψ_i using a robust Kohn–Sham inversion procedure [5]. For geometries close to perfect squares (D_{4h}), their inversion procedure fails to converge; i.e., occupation “holes” appear under the HOMO if single-determinant occupancies are enforced. Stable KS solutions are obtained *only if fractional* occupancies are allowed in (7). Geometries far from D_{4h} admit conventional integer-occupancy KS solutions. Standard exchange-correlation GGAs (Generalized Gradient Approximations) also produce fractional

occupancies near D_{4h} geometries, but with rather poor accuracy compared to the exact Kohn–Sham results [4].

In this chapter, a recently developed [6, 7] strong-correlation density functional, “B13”, is benchmarked on the Schipper et al. [4] $H_2 + H_2$ data, and also on ethylene torsion and cyclobutadiene automerization data from Jiang et al. [8]. All three of these are challenging avoided-crossing problems involving fractional occupancies near their transition states. The B13 functional is reviewed in Sect. 2. Variational optimization of B13 fractional occupancies, and reaction profiles for our three avoided-crossing tests, are discussed in Sect. 3. Dissociation curves for the single bonds H_2 and LiH are presented in Sect. 4. Concluding remarks and future prospects are discussed in Sect. 5.

2 The B13 Strong-Correlation Density Functional

In recent papers [6, 7] we have introduced a correlation-energy density functional able to describe both moderately and strongly correlated systems. “Strong” correlation arises from a small HOMO–LUMO gap, resulting in strong mixing of the configurations

$$|\cdots\psi_{\text{HOMO}}^2\psi_{\text{LUMO}}^0\rangle \text{ and } |\cdots\psi_{\text{HOMO}}^0\psi_{\text{LUMO}}^2\rangle \quad (8)$$

as described above. The signature of strong correlation in KS-DFT is *fractional occupancies* in the minimum-energy KS density (see (7)). At the same time, Janak’s theorem [3, 9] implies that

$$e_{\text{HOMO}} = e_{\text{LUMO}} \quad (9)$$

in any such strongly-correlated, fractionally-occupied, Kohn–Sham minimum.

Strong correlation is often discussed in the context of molecular bond dissociation; i.e., the correlation energy required to dissociate molecular bonds using *spin-restricted* orbitals. Small HOMO–LUMO gaps and strong mixing of configurations play a major role here as well. Spin-restricted dissociation of molecules implies

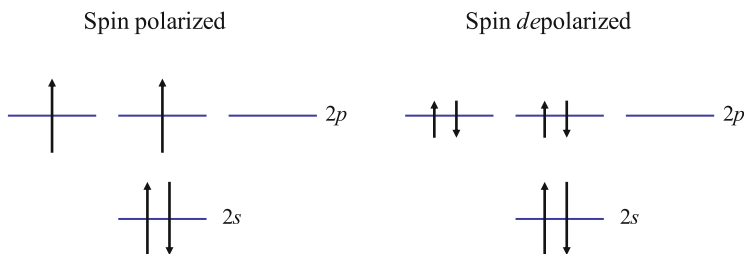


Fig. 2 Carbon atom spin states

that, for *all free atoms*, the usual Hund’s-rule spin-polarized configuration has the *same energy* as the spin-depolarized configuration obtained by replacing every unpaired electron by half an electron of spin up and half an electron of spin down (as sketched for the carbon atom in Fig. 2). This is a stringent test of density functionals. Conventional GGAs fail this test [7] with errors of the order of 40 kcal/mol in the first three rows of the periodic table. Our B13 functional, however, is designed to capture this spin-invariance property [7] while maintaining good performance in standard thermochemical applications.

B13 is based on *exact* exchange and is hence a *pure correlation* theory. The total exchange-correlation energy has the form [6, 7]

$$E_{XC}^{B13} = E_X^{\text{exact}} + E_C^{B13} + \Delta E_{\text{strong C}}^{B13} \quad (10)$$

where E_X^{exact} is the exactly-computed Kohn–Sham (or Hartree–Fock depending on the implementation) exchange energy, E_C^{B13} is a sum of opposite- and parallel-spin *static* and *dynamical* correlation potential energies:

$$E_C^{B13} = a_{\text{stat C}}^{\text{opp}} U_{\text{stat C}}^{\text{opp}} + a_{\text{stat C}}^{\text{par}} U_{\text{stat C}}^{\text{par}} + a_{\text{dyn C}}^{\text{opp}} U_{\text{dyn C}}^{\text{opp}} + a_{\text{dyn C}}^{\text{par}} U_{\text{dyn C}}^{\text{par}} \quad (11)$$

and $\Delta E_{\text{strong C}}^{B13}$ is a *strong-correlation correction* given by

$$\Delta E_{\text{strong C}}^{B13} = \sum_{n=2}^N c_n \int x^n u_C d^3r. \quad (12)$$

To an excellent first approximation, the four prefactors in (11) are all equal to each other with optimum value 0.62 (see Becke [6]). Nevertheless, greater accuracy can be achieved by fitting these independently. In (12), u_C is the sum of the *integrands* of the four terms in (11):

$$u_C = u_{\text{stat C}}^{\text{opp}} + u_{\text{stat C}}^{\text{par}} + u_{\text{dyn C}}^{\text{opp}} + u_{\text{dyn C}}^{\text{par}}, \quad (13)$$

namely the static + dynamical correlation potential-energy *density*, and x is the following ratio of the *static* correlation potential-energy density to the total:

$$x = \frac{u_{\text{stat C}}^{\text{opp}} + u_{\text{stat C}}^{\text{par}}}{u_C}. \quad (14)$$

This is a reasonable, local measure of strong correlation. In atoms, where strong correlation is insignificant, $x \rightarrow 0$. In stretched, spin-restricted H_2 , on the other hand, the quintessential case of strong correlation, $x \rightarrow 1$. We assume that intermediate situations are well characterized by intermediate values of x . The c_n in (12) are polynomial expansion coefficients fit to the atomic spin-depolarization condition of the previous paragraph.

Our fit set in Becke [7] consisted of the “G2/97” atomization energies of Curtiss, Raghavachari, and Pople [10] plus the spin-depolarization condition on all open-shell atoms $Z < 36$, including transition metal atoms. Two terms were deemed optimum in the strong-correlation correction, (12). The best-fit coefficients are

$$\begin{aligned} c_{\text{stat C}}^{\text{opp}} &= 0.552 & c_{\text{stat C}}^{\text{par}} &= 0.844 \\ c_{\text{dyn C}}^{\text{opp}} &= 0.640 & c_{\text{dyn C}}^{\text{par}} &= 0.559 \\ c_2 &= 0.825 & c_3 &= -0.380 \end{aligned} \quad (15)$$

and these are used in the present work. Mean absolute B13 errors on the G2/97 atomization energies and the atomic spin-depolarization tests are 3.8 and 5.7 kcal/mol, respectively [7].

It should be noted that the B13 correlation model is based on a *single* Slater determinant as the reference state [6]. The model adds multi-center correlations to *single*-determinantal pair densities as the starting point. How then, can B13 be justified in fundamentally two-configuration problems such as avoided crossings? Consider again the 50/50 mixtures at symmetric avoided-crossing transition states [11]. Imagine replicating the system of interest by an identical system at infinite distance from the first. The degenerate orbitals ψ_a and ψ_b on the system (*A*) and its replicant (*B*) combine to form the degenerate “super” system orbitals

$$\psi_{a\pm}^{\text{super}} = \frac{1}{\sqrt{2}}(\psi_a^A \pm \psi_a^B) \quad \text{and} \quad \psi_{b\pm}^{\text{super}} = \frac{1}{\sqrt{2}}(\psi_b^A \pm \psi_b^B). \quad (16)$$

Now consider the *single* supersystem Slater determinant with occupancy

$$|\cdots \psi_{a+}^{\text{super}}(\uparrow\downarrow) \psi_{b+}^{\text{super}}(\uparrow\downarrow)\rangle. \quad (17)$$

In each *subsystem*, this determinant places *one* electron in ψ_a (half spin-up and half spin-down) and similarly *one* electron in ψ_b , precisely the density of (6) corresponding to a 50/50 configuration mixture.

The more general densities of (7) can be reproduced by single Slater determinants spanning supersystems of *more* than two replicas. Appropriate numbers of replicants and appropriate occupations of supersystem orbitals can reproduce *any* two-configuration density. Because B13 *maximizes* multi-center correlation, it delivers the *ground state* energy corresponding to any such two-configuration density, *not* an excited-state energy or an ensemble energy. Excited states supported by the HOMO–LUMO orbitals will be studied in future work.

3 Avoided-Crossing Reaction Curves

In Becke [11], B13 was tested on barrier heights of four symmetric avoided-crossing reactions: H_4 , ethylene double-bond twisting, and double-bond automerization in cyclobutadiene and cyclooctatetraene. At the transition states of these reactions, there is 50/50 HOMO–LUMO mixing by symmetry. Variational determination of fractional occupancies was not needed. In this chapter, however, we draw full reaction curves for the first three of these reactions. Thus fractional occupancies must be computed.

Self-consistent B13 calculations are not yet possible, though prospects for SCF-B13 are good; see Proynov et al. [12–14] for an SCF implementation, and Arbuznikov and Kaupp [15] for an OEP implementation of an earlier B13 variant known as B05 [16]. Our current calculations are “post-LDA.” All total energies are evaluated using LDA orbitals computed by the grid-based NUMOL program [17, 18]. The optimum post-LDA fractional occupancies in (7) are determined by searching in the range $0 \leq f \leq 1$ for the minimum-energy f value. We adopt the simple strategy of minimizing the energy of a three-point quadratic interpolation with calculations performed at $f = 0, 1/2$, and 1. For comparison purposes, the same post-LDA three-point approach is applied to the B88 [19]+PBE [20] exchange-correlation GGA.

In our first avoided-crossing reaction, $H_2 + H_2$, we consider the nine H_4 geometries in Table II of Schipper et al. [4]. Each geometry is a rectangle with the longer side denoted R and the shorter side denoted r . Table 1 lists these geometries, along with the fractional occupancies f for “exact” Kohn–Sham, for the B88+PBE exchange-correlation GGA, and for B13. We find qualitative agreement between our B88+PBE GGA results and the B88+LYP [21] GGA results in Schipper et al. [4] (also recorded in Table 1), but both GGA sets agree poorly with exact Kohn–Sham. There is qualitative agreement, however, between our B13 fractional occupancies and the exact KS values, although B13 appears to be somewhat too strongly correlated. Note that the region of fractional occupancies near the square

Table 1 Fractional occupancies as in (7) for the $H_2 + H_2$ reaction

R	r	Exact KS	B88+LYP	B88+PBE	B13
2.32	2.32	0.50	0.50	0.50	0.50
2.35	2.29	0.32	0.10	0.07	0.45
2.40	2.21	0.07	0.00	0.00	0.33
2.50	2.06	0.00	0.00	0.00	0.11
2.75	1.68	0.00	0.00	0.00	0.00
3.00	1.44	0.00	0.00	0.00	0.00
4.00	1.41	0.00	0.00	0.00	0.00
5.00	1.40	0.00	0.00	0.00	0.00
10.0	1.40	0.00	0.00	0.00	0.00

Geometry parameters R and r in bohr. Exact KS and B88+LYP results from Schipper et al. [4]. B88+PBE and B13 results from the present work

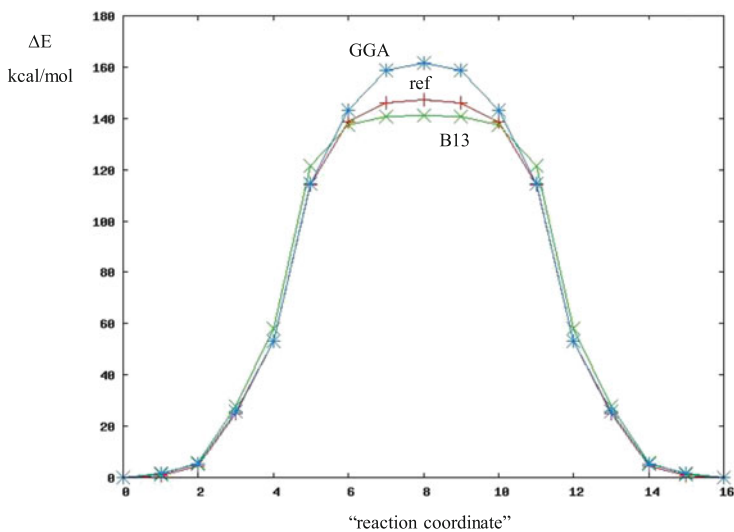


Fig. 3 Reaction profile for $H_2 + H_2$

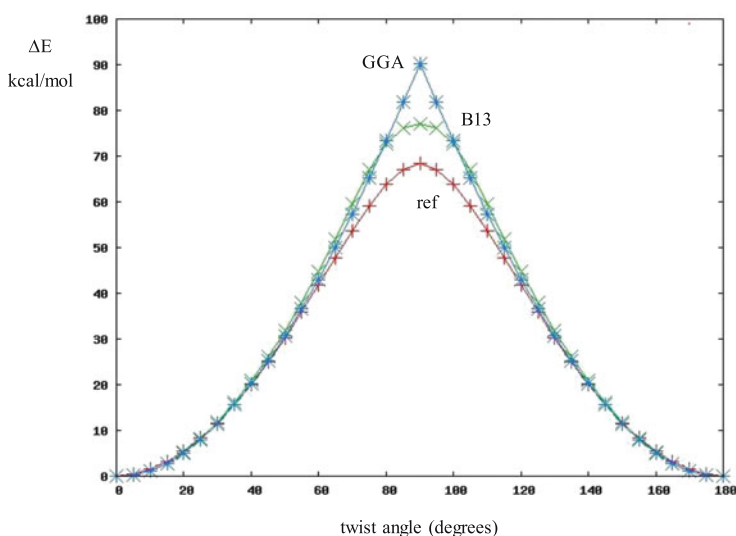


Fig. 4 Reaction profile for ethylene twist

transition state is smaller for the GGA than for exact KS and B13. The exact KS, GGA, and B13 energy curves are plotted in Fig. 3. The energy zero for each curve is the energy at geometry $R = 10.0$ and $r = 1.40$ bohr. The B13 reaction barrier of 141.2 kcal/mol is in fair agreement with the MRCI barrier of 147.6 kcal/mol.

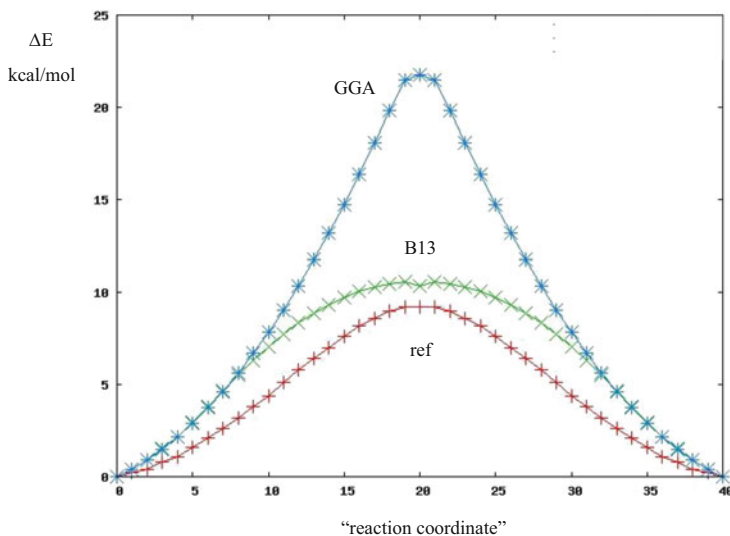


Fig. 5 Reaction profile for cyclobutadiene automerization

Our second avoided-crossing test is twisting around the double bond in ethylene. We took MR-ccCA (Multi-Reference Correlation Consistent Composite Approach) reference data from Jiang, Jeffrey, and Wilson [8] and have performed all calculations at the geometries specified in their paper. Figure 4 plots reference, B88 + PBE GGA, and B13 reaction curves. Zero energy for each method is the planar ethylene equilibrium geometry. In this case, the GGA energies always minimize at $f=0$ (no HOMO–LUMO mixing) producing an unphysical cusp at the top of the GGA curve. The B13 curve, on the other hand, is smooth throughout. The B13 barrier of 77.1 kcal/mol agrees better with the MR-ccCA barrier of 68.3 kcal/mol than does the GGA barrier, 90.2 kcal/mol.

Double-bond automerization in cyclobutadiene is an especially challenging avoided-crossing test. The reaction profile is plotted in Fig. 5, with MR-ccCA reference data and geometries again from Jiang, Jeffrey, and Wilson [8]. Zeroes of all curves correspond to the rectangular equilibrium geometry. The GGA curve is cuspless in this case but has a barrier more than twice too large (21.8 kcal/mol compared to 9.2 kcal/mol for MR-ccCA). The B13 barrier of 10.4 kcal/mol compares quite well with the 9.2 kcal/mol MR-ccCA barrier.

4 H₂ and LiH Dissociation Curves

Spin-restricted KS-DFT dissociation curves, even employing sophisticated GGA and hybrid functionals, have asymptotes well above the exact dissociation limits. Spin-*un*restricted calculations (“UKS”) can capture the correct limits. UKS

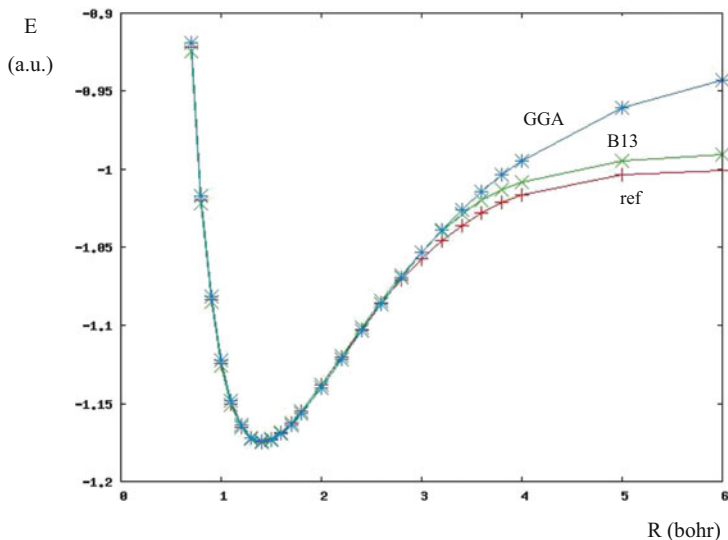


Fig. 6 H_2 dissociation

computations are undesirable, however, as they break spin and space symmetries. To the best of our knowledge, no successful spin-restricted DFT dissociation curve has yet been reported in the literature. We therefore apply B13 to this fundamental problem.

In Fig. 6 the H_2 dissociation curve is plotted for highly accurate Hylleraas variational reference data from Sims and Hagstrom [22] for the B88+PBE GGA and for B13. Fractional mixing of the σ_g and the σ_u orbitals begins at $R \sim 3.4$ bohr for B13. The GGA does not mix these orbitals at all, and the GGA curve is significantly above the exact asymptote. B13, on the other hand, exhibits a good dissociation limit and, quite interestingly, an asymptotic f of 0.50 (computed at $R = 30.0$ bohr), in accord with the asymptotic CI wavefunction

$$\frac{1}{\sqrt{2}} \left(|\sigma_g^2\rangle - |\sigma_u^2\rangle \right). \quad (18)$$

That B13 is sensitive enough to mix these MOs, and with the correct mixing fraction no less, is intriguing.

The heteronuclear dissociation of LiH is even more interesting. At large separation, the HOMO of the system is the 1s orbital of the H atom, and the LUMO is the 2s orbital of the Li atom. Thus the two configurations

$$|1s_{Li}^2 \cdot \text{HOMO}^2\rangle \text{ and } |1s_{Li}^2 \cdot \text{LUMO}^2\rangle \quad (19)$$

have charges Li^+H^- and Li^-H^+ and dissociation to neutral atoms requires $f=0.50$. Because LDA calculations on Li^- and H^- are problematic, the $f=0$ and $f=1$

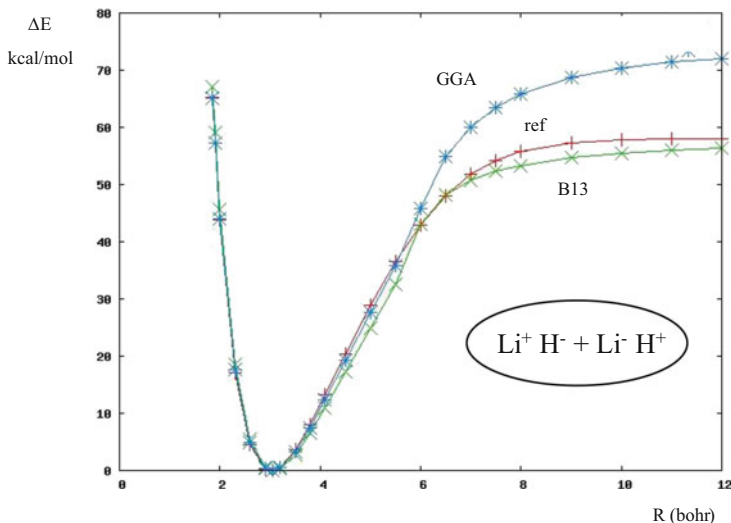


Fig. 7 LiH dissociation

endpoints of the quadratic minimization are unreliable at large separations. Instead, we scan over f values in steps of 0.05 in order to locate the energy minimum at each internuclear separation.

We plot LiH dissociation curves for MR-CISD (Multi-Reference Configuration Interaction with Singles and Doubles) reference data [23], the B88 + PBE GGA, and B13 in Fig. 7. All curves are zeroed at their minimum energy. The limit of the GGA dissociation curve is too high. The B13 curve has an excellent asymptotic energy, and an asymptotic f (computed at $R = 80.0$ bohr) of 0.45, very close to the required 0.50. The dissociation limit is roughly $\text{Li}^{+0.1}\text{H}^{-0.1}$, very close to neutral atoms. The manner in which B13 captures, to a very good approximation, the correct dissociation limit of this heteronuclear bond is fascinating. At play is a “resonance” of singlet ionic atomic states.

5 Summary and Conclusions

This work marks the first successful application of a spin-restricted Kohn–Sham density functional, “B13”, to two-configuration mixing problems with densities as in (7). Moreover, B13 is *exact-exchange*-based. Therefore stretched radical systems such as H_2^+ and He_2^+ , the bane of GGA and hybrid functionals [24], are correctly accommodated.

These calculations have been post-LDA and not self-consistent. It is difficult to predict how self-consistency might change their nature, and what significance would be lent to the orbital energies. Is the HOMO–LUMO mixing in H_2 and

LiH an artifact of the post-LDA approach here? Might mixing be obviated in an SCF approach? SCF implementations of the predecessor “B05” functional have been published [12–15]. SCF-B13 should be possible too and could be very interesting.

In future work we will also investigate *multiple* bond dissociations and other strongly-correlated reactions requiring variational optimization of one *or more* mixing fractions. Low-lying *excited* states of strongly-correlated systems, and how they might depend on B13 ground-state determinations, will be explored as well.

The author gratefully acknowledges the Natural Sciences and Engineering Research Council (NSERC) of Canada for research support, the Killam Trust of Dalhousie University for salary support through the Killam Chair program, and the Atlantic Computational Excellence network (ACEnet) for computing support.

References

1. Hohenberg P, Kohn W (1964) Phys Rev 136:B864
2. Kohn W, Sham LJ (1965) Phys Rev 140:A1133
3. Parr RG, Yang W (1989) Density-functional theory of atoms and molecules. Oxford University Press, New York
4. Schipper PRT, Griitsenko OV, Baerends EJ (1999) J Chem Phys 111:4056
5. Schipper PRT, Griitsenko OV, Baerends EJ (1997) Theor Chem Acc 98:16
6. Becke AD (2013) J Chem Phys 138:074109
7. Becke AD (2013) J Chem Phys 138:161101
8. Jiang W, Jeffrey CC, Wilson AK (2012) J Phys Chem A 116:9969
9. Janak JF (1978) Phys Rev B 18:7165
10. Curtiss LA, Raghavachari K, Redfern PC, Pople JA (1997) J Chem Phys 106:1063
11. Becke AD (2013) J Chem Phys 139:021104
12. Proynov E, Shao Y, Kong J (2010) Chem Phys Lett 493:381
13. Proynov E, Liu F, Kong J (2012) Chem Phys Lett 525:150
14. Proynov E, Liu F, Shao Y, Kong J (2012) J Chem Phys 136:034102
15. Arbuznikov AV, Kaupp M (2009) J Chem Phys 131:084103
16. Becke AD (2005) J Chem Phys 122:064101
17. Becke AD (1989) Int J Quantum Chem Quantum Chem Symp 23:599
18. Becke AD, Dickson RM (1990) J Chem Phys 92:3610
19. Becke AD (1988) Phys Rev A 38:3098
20. Perdew JP, Burke K, Ernzerhof M (1996) Phys Rev Lett 77:3865
21. Lee C, Yang W, Parr RG (1988) Phys Rev B 37:785
22. Sims JS, Hagstrom SA (2006) J Chem Phys 124:094101
23. Holka F, Szalay PG, Fremont J, Rey M, Peterson KA, Tyuterev VG (2011) J Chem Phys 134:094306
24. Becke AD (2003) J Chem Phys 119:2972